CO Adsorption on Defective Graphene-Supported Pt13 Nanoclusters

ARTICLE *in* THE JOURNAL OF PHYSICAL CHEMISTRY C · OCTOBER 2013

Impact Factor: 4.77 · DOI: 10.1021/jp403468h

2 AUTHORS, INCLUDING:

Ioanna Fampiou
University of Delaware
9 PUBLICATIONS **96** CITATIONS

SEE PROFILE

THE JOURNAL OF PHYSICAL CHEMISTRY C

Article

pubs.acs.org/JPCC

CO Adsorption on Defective Graphene-Supported Pt_{13} Nanoclusters

Ioanna Fampiou and Ashwin Ramasubramaniam*

Department of Mechanical and Industrial Engineering, University of Massachusetts Amherst, Amherst, Massachusetts 01003, United States

ABSTRACT: Platinum (Pt) nanoclusters on graphene have been shown to possess superior catalytic activity and increased selectivity in a variety of electrochemical reactions compared with bulk Pt electrodes. In this work, we use density functional theory calculations to investigate the adsorption of CO on low-energy Pt_{13} clusters bound at various point defects in graphene. The presence of dangling bonds at defects in the graphene support leads to strong Pt−carbon bonding and a commensurate downshift of the cluster *d*-band center. This downshift of the *d*-band in turn decreases the binding energy of CO molecules to the cluster. Systematic random sampling of CO adsorption on clusters bound at various defects in graphene reveals that supported clusters, on average, bind CO more weakly than unsupported clusters. Moreover, the adsorption energies of CO on defective-graphene-supported clusters are found to be comparable with reported adsorption energies at undercoordinated sites, such as step-edges, on low-index Pt surfaces. Our results suggest that tailoring cluster−support interactions through defect engineering could provide a route for improving the tolerance of subnanometer Pt clusters to CO poisoning.

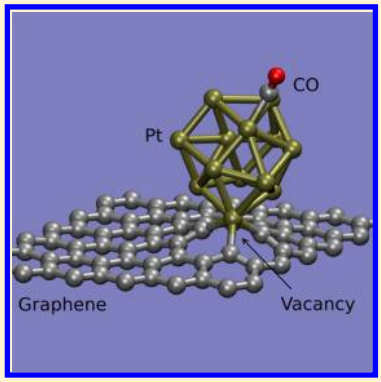

I. INTRODUCTION

Graphene-supported transition-metal nanoparticles have attracted considerable interest as electrocatalysts in direct methanol fuel cells, proton exchange membrane fuel cells, and hydrogen fuel cells.[1−10] For example, recent experiments in methanol fuel cells indicate that electrodes composed of Pt nanoclusters dispersed on chemically converted graphene exhibit a lower tendency for sintering, accompanied by high catalytic activity and tolerance to CO poisoning, rivaling that of state-of-the-art Pt−Ru electrocatalysts.[6−8,11,12] Of these studies, several have also shown that defects in graphene supports play a key role in stabilizing the catalyst nanoclusters against sintering by providing strong anchoring sites.[8,13,14] This has been corroborated by computational studies that report a strong energetic preference for binding of Pt clusters at defect sites in graphene relative to a pristine graphene sheet.[13−19] First-principles calculations also suggest that support defects can appreciably alter the morphology and electronic structure of clusters, most notably, causing a downshift of the Pt *d*-band center,[16,17,19−21] thereby improving their CO tolerance. The improved performance of Pt−graphene composite electrodes may then be attributed to several factors including (a) stability toward sintering, which maintains high surface area over extended periods, (b) improved electrical conductivity of graphene supports relative to standard carbon black counterparts, and (c) fundamental modifications in the electronic structure of the supported nanoparticle as a result of strong binding to support defects. The relative importance of these factors and their potentially synergistic interaction is still not fully understood and remains a matter of current interest.

The goal of this work is to systematically explore the interaction between various graphene point defects and Pt nanoclusters, and to quantify the effect of these interactions on the energetics of CO binding to the supported cluster. In the following, we focus on Pt_{13} nanoclusters and investigate, via first-principles density functional theory (DFT), the adsorption energetics of CO on free clusters as well as on clusters supported on pristine and defective graphene supports. The Pt_{13} clusters employed in our studies are optimized low-energy clusters with open, low-symmetry morphologies that were derived via the annealing and quenching method reported in our previous study;[17] these clusters are thermodynamically more stable than the high-symmetry icosahedral or octahedral Pt_{13} clusters. To account for the inherent statistical variability in the local environment of adsorption sites (symmetry-inequivalent on-top, hollow, and bridge sites) encountered by a CO molecule on a low-symmetry Pt_{13} cluster, we randomly sample the CO binding energy at several distinct sites (ranging from 9 to 14 sites) per cluster−defect combination. Our studies show that Pt_{13} clusters supported on defective graphene bind CO more weakly than their unsupported counterparts, the strength of CO binding being inversely correlated with the strength of cluster−support binding. While CO binding on defect-supported clusters is still stronger than on an ideal Pt(111) surface, a more realistic comparison with binding at undercoordinated sites, such as vacancies or step edges on Pt surfaces, results in nearly comparable binding energies. Overall, our results clearly indicate the propensity of defective graphene substrates to reduce the binding energy of CO molecules on Pt_{13} clusters, which could be an important mechanism through

Received: April 9, 2013
Revised: August 13, 2013
Published: September 9, 2013

   dx.doi.org/10.1021/jp403468h | *J. Phys. Chem. C* 2013, 117, 19927−19933

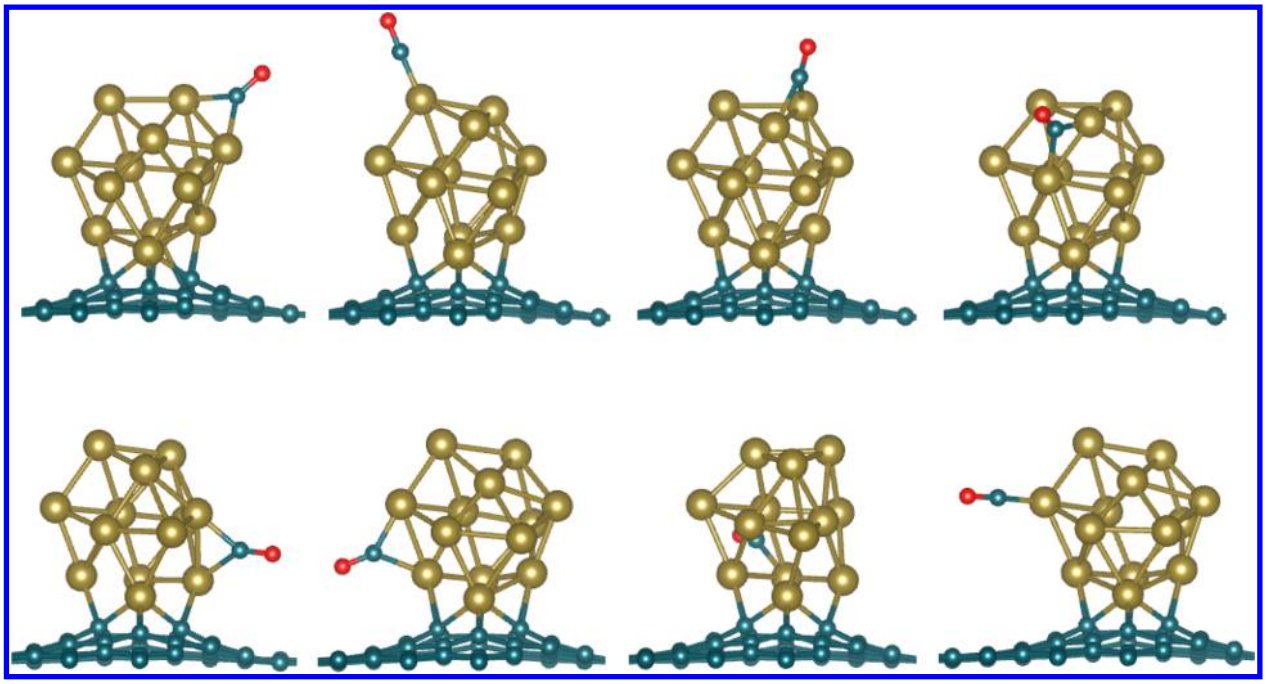

Figure 1. Sampled CO adsorption sites on a low-energy Pt_{13} cluster supported at a single vacancy in graphene. Cyan, gold, and red spheres represent C, Pt, and O atoms, respectively.

which graphene-supported Pt nanoclusters exhibit increased CO tolerance in experiments.

The remainder of this paper is organized as follows. In section II, we present computational details of our DFT calculations. Results and discussion on CO adsorption energetics are presented in section III. Concluding remarks are provided in section IV.

II. COMPUTATIONAL DETAILS

All calculations were performed with the plane-wave DFT method as implemented in the Vienna *ab initio* simulation package (VASP).[24,25] The projector-augmented wave (PAW) method[26,27] was used to describe the core and valence electrons. The Perdew–Burke–Ernzerhof[22] form of the generalized-gradient approximation was employed to describe electron exchange and correlation. All calculations were performed on a 6 × 6 graphene supercell with periodic boundary conditions; periodic images were separated by vacuum in excess of 15 Å normal to the sheets to prevent spurious image interactions. A kinetic energy cutoff of 400 eV was used in all structural relaxation simulations of CO adsorption, and the Brillouin zone was sampled using a 5 × 5 × 1 Γ-centered *k*-point mesh. Reference calculations for Pt(111) were performed on a four-layer, 4 × 4 slab with periodic boundary conditions in the plane of the surface. Atoms in the bottommost layer were fixed at their bulk positions while the top three layers were relaxed in all calculations. A kinetic energy cutoff of 400 eV was used in these slab calculations with a Γ-centered 7 × 7 × 1 *k*-point mesh for Brillouin-zone sampling. In all cases (slab and cluster), structural relaxations were performed using a conjugate gradient algorithm until forces on all atoms were below 0.01 eV/Å. To accelerate electronic convergence, a second-order Methfessel–Paxton[23] smearing of the Fermi surface was employed with a smearing width of 0.05 eV. All calculations were performed with spin polarization.

For supported-cluster studies, we employed the lowest-energy structures of graphene-supported Pt_{13} clusters derived via the annealing and quenching method reported in our previous study.[17] As described in that work, these structures also have lower energy, lower symmetry, and a more open morphology than the icosahedral or octahedral clusters that have commonly been used in DFT studies. To compare and contrast CO binding on supported versus free clusters, the low energy clusters were also removed from the graphene supports and employed in studies of CO adsorption (with full structural relaxation). This procedure allows us to directly address the effect of the support on CO binding.

Throughout this paper, we employ the adsorption energy (E_{ad}) of CO on graphene-supported as well as free Pt_{13} clusters as a metric for the strength of binding between CO and Pt, which is defined as

$$E_{ad} = \begin{cases} E_{C_m+Pt_{13}+CO} - E_{C_m+Pt_{13}} - E_{CO}, & \text{supported clusters} \\ E_{Pt_{13}+CO} - E_{Pt_{13}} - E_{CO}, & \text{free clusters} \end{cases} \quad (1)$$

where $E_{C_m+Pt_{13}+CO}$, $E_{C_m+Pt_{13}}$, $E_{Pt_{13}+CO}$, and E_{CO} are the total energies of the graphene–Pt_{13}–CO system, the graphene–Pt_{13} system, the CO–Pt_{13} system, and the CO molecule as obtained from DFT calculations. As defined here, more negative values of E_{ad} signify stronger binding.

III. RESULTS AND DISCUSSION

A. CO Adsorption on Free and Graphene-Supported Pt_{13} Clusters. First, we examine the adsorption of a single CO molecule on free and graphene-supported low-energy Pt_{13} clusters. On a planar surface such as Pt(111), it is relatively straightforward to identify via symmetry arguments a minimal set of binding sites (on-top, bridge, hollow sites) for CO adsorption studies. While similar on-top/bridge/hollow binding

dx.doi.org/10.1021/jp403468h | J. Phys. Chem. C 2013, 117, 19927–19933

sites can be identified on a Pt_{13} cluster such as the one displayed in Figure 1, reduced (or complete lack of) symmetry renders each of these sites unique; it is not feasible to sample each and every such site with DFT. To render this problem tractable while still accounting meaningfully for the inherent statistical variability in the nature of binding sites, we randomly sample between 9 and 14 different adsorption sites on every cluster. To further account for the influence of support defects on CO−Pt_{13} interactions, we sample over clusters supported on pristine graphene as well as on defective graphene containing a single vacancy, an unreconstructed divacancy, and a 555−777 divacancy reconstruction. Figure 1 shows some of the sampled CO adsorption sites for the case of a low-energy Pt_{13} cluster supported on graphene with single vacancy. Similar sampling procedures were followed for the other cases.

In Table 1, we report the average CO adsorption energy on graphene-supported and free Pt_{13} clusters, calculated according to eq 1. Statistical errors are estimated using a 95% confidence interval of the Student's t-distribution, which is appropriate for small-sample statistics. The average C−O bond lengths (d_{C-O}) for the adsorbed CO molecule are also reported here along with their statistical errors. Among the different CO adsorption sites studied on the Pt_{13} clusters, we found on average that CO tends to bind more strongly to on-top sites of the clusters whereas adsorption is generally weaker on hollow sites of the clusters. We do not find any obvious correlation between the binding energy of CO to the cluster relative to the distance of the binding site from the graphene substrate (i.e., toward the bottom or top of the cluster). The fully relaxed atomic structures for one selected case each of CO adsorption on supported clusters and free clusters are displayed in Figure 2.

Table 1. Average Adsorption Energy and Bond Lengths (d_{C-O}) for CO Molecules Adsorbed on Low-Symmetry Pt_{13} Clusters Supported on Pristine and Defective[a] Graphene, as well as on Free Pt_{13} Clusters[b]

graphene substrate	adsorption energy (eV)	d_{C-O} (Å)
pristine	−2.54 ± 0.19	1.18 ± 0.01
vacancy	−2.33 ± 0.11	1.18 ± 0.01
divacancy	−2.02 ± 0.18	1.18 ± 0.01
555−777	−2.24 ± 0.17	1.19 ± 0.01
free clusters	−2.79 ± 0.30	1.17 ± 0.01
Pt(111) (T)	−1.66	1.16
Pt(111) (V)	−2.21	1.18
Pt(111) (V-line)	−2.27	1.19

[a]Single vacancy, unreconstructed divacancy, and 555−777 reconstructed divacancy. [b]CO adsorption energies on Pt(111) at an on-top (T) site, a vacancy site (V), and a vacancy line (V-line) are reported for comparison. For reference, the C−O bond length in an isolated molecule is calculated to be 1.17 Å.

The CO adsorption energy results reported in Table 1 indicate that the presence of a point defect in the graphene substrate weakens the interaction of the CO molecule with the Pt_{13} clusters. In particular, for the three different defective graphene supports (single vacancy, unreconstructed divacancy, and 555−777 divacancy reconstruction), the CO adsorption energy on the Pt_{13} cluster is lower by 0.21 eV, 0.52 eV, and 0.30 eV, respectively, compared with the average adsorption energy on Pt_{13} clusters supported on defect-free pristine graphene; the difference in binding energies relative to unsupported Pt_{13} clusters is even larger (0.46 eV, 0.77 eV, and 0.55 eV, respectively). Previous reports[16,17,19−21] have correlated the presence of a point defect on the graphene support with stronger binding of the metal cluster. Here, another key role of the point defect in the graphene substrates is revealed: CO adsorption is less favorable on Pt_{13} clusters supported at defective graphene substrates compared with isolated Pt_{13} clusters. This result is particularly significant because it suggests that defect engineering of graphene substrates could improve the CO tolerance of extremely small Pt clusters. Examining the average C−O bond lengths (d_{C-O}) for the adsorbed CO molecule (Table 1), we notice that the C−O bond (1.17 Å for an isolated molecule) is slightly elongated by 0.01−0.02 Å for graphene-supported clusters relative to the unsupported ones.

The obvious question that needs to be addressed is how CO adsorption on Pt_{13} clusters compares with that on macroscopic Pt surfaces. We studied the adsorption of a single CO molecule at the experimentally preferred on-top (T) site of the Pt(111) surface[46] and computed an adsorption energy of −1.66 eV (Table 1); the CO molecule is thus more weakly bound to an ideal Pt(111) surface than to any Pt_{13} cluster (supported or

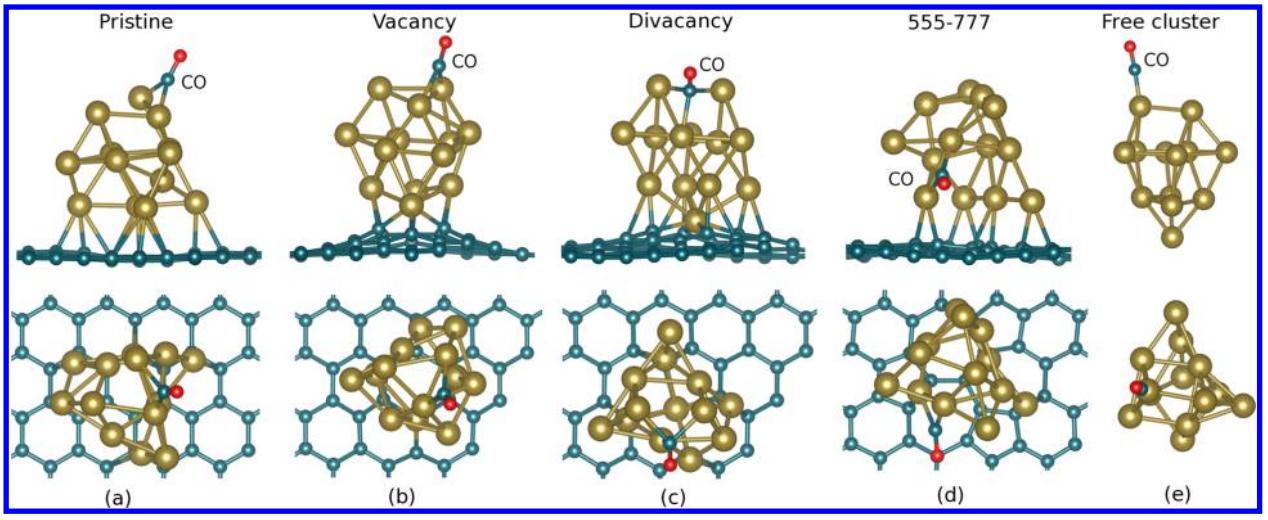

Figure 2. Side and top view of selected low-energy DFT configurations for adsorption of a CO molecule on graphene-supported Pt_{13} clusters. Cyan, gold, and red spheres represent C, Pt, and O atoms, respectively.

dx.doi.org/10.1021/jp403468h | J. Phys. Chem. C 2013, 117, 19927−19933

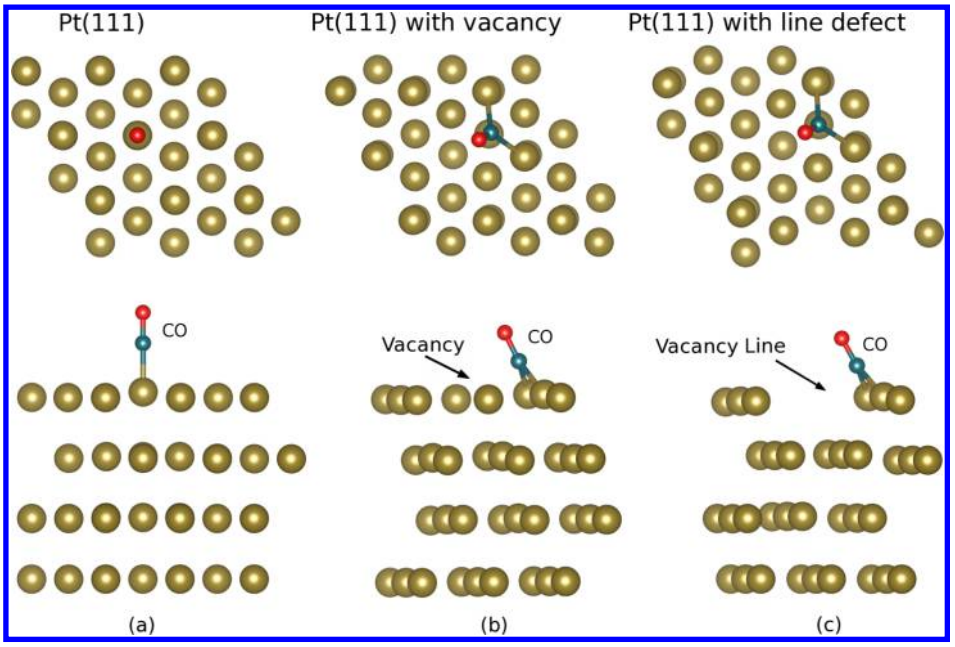

Figure 3. Side and top view of DFT configurations for adsorption of a CO molecule on Pt(111) surface slabs. Cyan, gold, and red spheres represent C, Pt, and O atoms, respectively.

otherwise). A more realistic estimate for a Pt electrode should, at the very least, account for the presence of surface defects (vacancies/adatoms/step-edges/kinks) as well as other crystalline orientations. To ascertain, at least approximately, the energetics of binding at undercoordinated sites, we also examined CO binding to a single vacancy and to a vacancy line (which is a rough approximation of a step-edge) on Pt(111) (Figure 3) and computed adsorption energies of −2.21 eV and −2.27 eV, respectively. Binding to these surface defects is then energetically comparable to that on defective graphene-supported Pt_{13} clusters (Table 1). While detailed studies of CO adsorption on other crystalline facets is beyond the scope of this work, we note for comparison some relevant studies from the literature. DFT studies report that CO binds more strongly to step-edges on Pt(211) surfaces compared with terrace sites of both the Pt(211) and the flat Pt(111) surface,[28,29] with adsorption energies in the range of −1.95 to −2.49 eV. Orita and Inada[30] found that CO binds preferentially at a step-edge on the Pt(211) surface with an adsorption energy of −2.41 eV, and at the step-edge of an unreconstructed Pt(311) surface with an adsorption energy of −2.43 eV. Yamagishi, Fujimoto, Inada, and Orita[31] reported that CO binds at a step-edge on a Pt(410) surface with an adsoprtion energy of −2.49 eV and at a step-edge on a Pt(110) surface with adsorption energy of −2.36 eV. These studies, in conjunction with the two cases of a defective Pt(111) surface considered here, indicate that a CO molecule, on average, is adsorbed at least as strongly to undercoordinated Pt surface sites as to defective graphene-supported Pt_{13} clusters. Unsupported Pt_{13} clusters, however, bind CO more strongly than in any of the above cases. Thus, our results suggest that defective graphene supports can indeed play a role in mitigating CO poisoning of subnanometer Pt clusters.

B. Electronic Structure of CO Bound on Graphene-Supported and Free Pt_{13} Clusters. Next, we analyze the electronic structure of the graphene−Pt_{13} cluster−CO systems for the four different types of graphene supports, as well as the free Pt_{13} cluster−CO systems. In our previous study of graphene-supported Pt_{13} clusters,[17] we showed a clear correlation between the position of the *d*-band center of the bound cluster and the nature of the support point defect. Specifically, stronger binding of the cluster to the defect (which is directly related to the number of dangling bonds at the defect) is accompanied by increased charge transfer from the cluster to the substrate and a shift of the cluster *d*-band center away from the Fermi level. In Figure 4, we correlate this *d*-band shift, which is effectively a surrogate for the type of binding defect, to the average CO adsorption energy. As seen from this figure, the position of the cluster *d*-band center is well correlated with the CO adsorption energy: the further away the *d*-band center is from the Fermi level, the weaker is the CO adsorption energy.[32−35] This could provide a credible explanation for experimental observations of increased CO

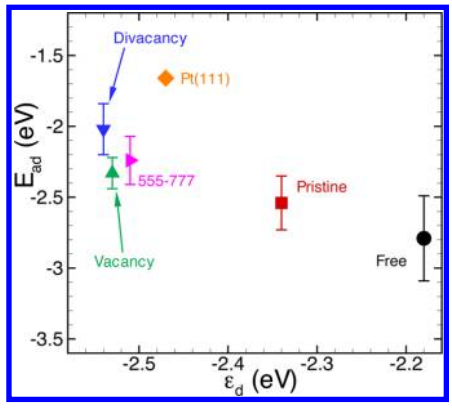

Figure 4. CO adsorption energy (E_{ad}) as a function of *d*-band center (ε_d) relative to the Fermi energy for supported Pt_{13} clusters, free Pt_{13} clusters, and Pt(111) surface. A downshift of the cluster *d*-band center with respect to the Fermi level (more negative ε_d) is directly correlated with weaker adsorption of CO on the cluster. Error bars indicate 95% confidence intervals obtained from sampling over multiple adsorption sites on the cluster.

dx.doi.org/10.1021/jp403468h | J. Phys. Chem. C 2013, 117, 19927−19933

tolerance[6−8,11,12] exhibited by Pt nanoparticles on chemically converted graphene or graphene oxide supports, which are inherently defective, unlike exfoliated graphene.

For all the cases of CO adsorption on graphene-supported and free Pt_{13} clusters, a Bader analysis[36,37] was performed, partitioning the total charge density between atoms, which then allowed us to quantify the total charge transfer between the cluster, CO molecule, and graphene support. The average charge transfer, Δq, between these constituents is reported in Table 2. We consistently find an appreciable net charge transfer from the Pt_{13} cluster to both the graphene support and the CO molecule. There is also significant redistribution of charge within the cluster and CO molecule, as well as in the immediate vicinity of the cluster within the graphene sheet, as seen clearly in the charge-density difference plots for select cases (Figure 5). The yellow and blue regions in these plots indicate the areas of charge accumulation and depletion, respectively. The adsorption of the CO molecule itself induces fairly localized charge redistribution in the immediate vicinity of the adsorption site as seen from the case of CO adsorption on the free cluster. The amount of charge transferred from the Pt cluster to CO (~0.25e^-; ~0.12e^- to C and ~0.13e^- to O) is also essentially independent of the cluster interaction with graphene. The charge transferred from the Pt cluster to graphene is, however, quite sensitive to nature of the support. A cluster adsorbed on pristine graphene transfers some charge to the support (~0.1e^-), but this is relatively small compared with the charge transfer from a cluster to a defective substrate (~0.2 − 0.8 eV). It is this substantial depletion of charge from the cluster to the defective support that leads to a downshift of the Fermi energy,[17] which in turn leads to weaker CO binding to the cluster as was alluded to before.

Table 2. Average Charge Transfer [Δq (e^-)] from the Pt_{13} Cluster to CO and Pristine Graphene, Single Vacancy, Unreconstructed Divacancy, and 555-777 Reconstructed Divacancy Based on Bader Analysis[a]

	Δq (e^-)		
	substrate	cluster	CO
pristine	0.09 ± 0.02	−0.35 ± 0.04	0.25 ± 0.03
vacancy	0.44 ± 0.01	−0.70 ± 0.02	0.26 ± 0.02
divacancy	0.76 ± 0.02	−1.01 ± 0.04	0.25 ± 0.03
555−777	0.26 ± 0.03	−0.52 ± 0.03	0.26 ± 0.03
free clusters		−0.24 ± 0.03	0.24 ± 0.03

[a]Positive/negative numbers indicate accumulation/depletion of electrons.

IV. CONCLUSIONS

In conclusion, DFT calculations were employed to investigate the adsorption of CO on Pt_{13} clusters supported on defect-free and defective graphene substrates, as well as unsupported clusters. Pt_{13} clusters were found to bind strongly to defects in graphene and correspondingly bind CO molecules more weakly compared with clusters supported on pristine graphene. In all cases, graphene-supported Pt_{13} clusters were found to bind CO more weakly than unsupported Pt_{13} clusters. These observations were explained in terms of the downshift of the *d*-band center position of the clusters upon binding to defects: stronger binding leads to greater charge transfer from the cluster to the substrate accompanied by a greater downshift of the *d*-band center. Consequently, the probe CO molecule binds more weakly to the cluster. While an ideal Pt(111) surface was found to bind CO more weakly than any of the Pt_{13} clusters studied here (supported or unsupported), binding to defects to the Pt(111) and other low-index surfaces is of comparable magnitude to that on supported Pt_{13} clusters. Overall, our study suggests that defect-engineered graphene not only can serve as robust support that strongly binds and stabilizes clusters against sintering but also might allow for optimizing catalytic properties through tuning of cluster−substrate interactions. Additional investigations of CO oxidation kinetics are needed to verify that such cluster−substrate interactions can also substantially influence the removal of CO thereby mitigating catalyst poisoning.

AUTHOR INFORMATION

Corresponding Author

*E-mail: ashwin@engin.umass.edu.

Notes

The authors declare no competing financial interest.

ACKNOWLEDGMENTS

This work was supported by the U.S. Department of Energy under Award Number DE-SC0010610.

REFERENCES

(1) Qiu, J. D.; Wang, G.-C.; Liang, R.-P.; Xia, X.-H.; Yu, H.-W. Controllable Deposition of Platinum Nanoparticles on Graphene As an Electrocatalyst for Direct Methanol Fuel Cells. *J. Phys. Chem. C* **2011**, *115*, 15639−15645.

(2) Auer, E.; Freund, A.; Pietsch, J.; Tacke, T. Carbons as Supports for Industrial Precious Metal Catalysts. *Appl. Catal., A* **1998**, *173*, 259−271.

(3) Planeix, J. M.; Coustel, N.; Coq, B.; Brotons, V.; Kumbhar, P. S.; Dutartre, R.; Geneste, P.; Bernier, P.; Ajayan, P. M. Application of

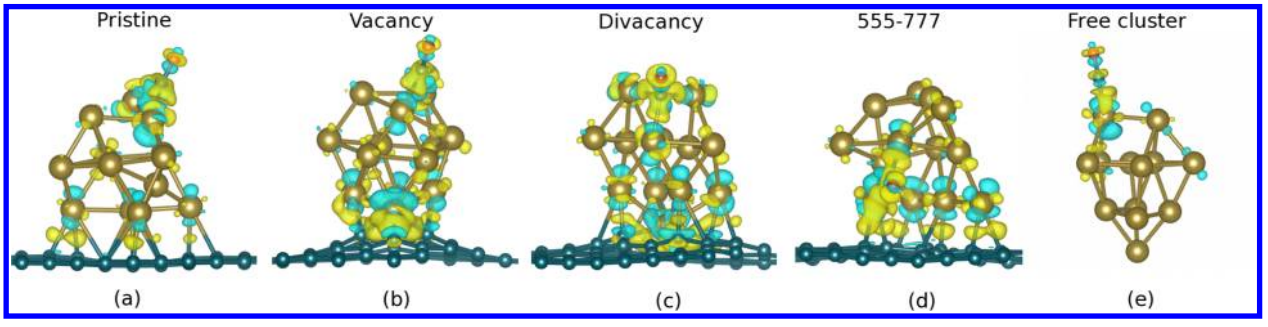

Figure 5. Charge-density difference plots for the selected DFT configurations of Figure 2. Isosurfaces are at 0.054 e/Å^3; yellow (blue) color represents charge accumulation (depletion).

Carbon Nanotubes as Supports in Heterogeneous Catalysis. *J. Am. Chem. Soc.* **1994**, *116*, 7935−7936.
(4) Tang, H.; Chen, J. H.; Nie, L. H.; Liu, D. Y.; Deng, W.; Kuang, Y. F.; Yao, S. Z. High Dispersion and Electrocatalytic Properties of Platinum Nanoparticles on Graphitic Carbon Nanofibers (GCNFs). *J. Colloid Interface Sci.* **2004**, *269*, 26−31.
(5) Kongkanand, A.; Kuwabata, S.; Girishkumar, G.; Kamat, P. Single−Wall Carbon Nanotubes Supported Platinum Nanoparticles with Improved Electrocatalytic Activity for Oxygen Reduction Reaction. *Langmuir* **2006**, *22*, 2392−2396.
(6) Yoo, E.; Okata, T.; Akita, T.; Kohyama, M.; Nakamura, J.; Honma, I. Enhanced Electrocatalytic Activity of Pt Subnanoclusters on Graphene Nanosheet Surface. *Nano Lett.* **2009**, *9*, 2255−2259.
(7) Li, Y.; Gao, W.; Ci, L.; Wang, C.; Ajayan, P. M. Catalytic Performance of Pt Nanoparticles on Reduced Graphene Oxide for Methanol Electro-oxidation. *Carbon* **2010**, *48*, 1124−1130.
(8) Kou, R.; Shao, Y.; Wang, D.; Engelhard, M. H.; Kwak, J. H.; Wang, J.; Viswanathan, V. V.; Wang, C.; Lin, Y.; Wang, Y.; et al. Enhanced Activity and Stability of Pt Catalysts on Functionalized Graphene Sheets for Electrocatalytic Oxygen Reduction. *Electrochem. Commun.* **2009**, *11*, 954−957.
(9) Seger, B.; Kamat, P. V. Electrocatalytically Active Graphene-Platinum Nanocomposites. Role of 2D Carbon Support in PEM Fuel Cells. *J. Phys. Chem. C* **2009**, *113*, 7990−7995.
(10) Zhong, J.; Nackashi, D.; Lu, W.; Kittrell, C.; Tour, J. M. Decoration, Migration, and Aggregation of Palladium Nanoparticles on Graphene Sheets. *Chem. Mater.* **2010**, *22*, 5695−5699.
(11) Yoo, E.; Okada, T.; Akita, T.; Kohyama, M.; Honma, I.; Nakamura, J. Sub-nano-Pt Cluster Supported on Graphene Nanosheets for CO Tolerant Catalysts in Polymer Electrolyte Fuel Cells. *J. Power Sources* **2011**, *196*, 110−115.
(12) Scheuermann, G. M; Rumi, L.; Steurer, P.; Bannwarth, W.; Mulhaupt, R. Palladium Nanoparticles on Graphite Oxide and Its Functionalized Graphene Derivatives as Highly Active Catalysts for the Suzuki−Miyaura Coupling Reaction. *J. Am. Chem. Soc.* **2009**, *131*, 8262−8270.
(13) Kou, R.; Shao, Y.; Mei, D.; Nie, Z.; Wang, D.; Wang, C.; Viswanathan, V. V.; Park, S.; Aksay, I. A.; Lin, Y.; et al. Stabilization of Electrocatalytic Metal Nanoparticles at Metal−Metal Oxide−Graphene Triple Junction Points. *J. Am. Chem. Soc.* **2011**, *133*, 2541−2547.
(14) Vedala, H.; Sorescu, D. C.; Kotchey, G. P.; Star, A. Chemical Sensitivity of Graphene Edges Decorated with Metal Nanoparticles. *Nano Lett.* **2011**, *11*, 2342−2347.
(15) Kong, K.; Choi, Y.; Ryu, B.-H.; Lee, J.; Chang, H. Investigation of Metal/carbon-related Materials for Fuel Cell Applications by Electronic Structure Calculations. *Mater. Sci. Eng., C* **2006**, *26*, 1207−1210.
(16) Okamoto, Y. Density-functional Calculations of Icosahedral M_{13} (M=Pt and Au) Clusters on Graphene Sheets and Flakes. *Chem. Phys. Lett.* **2006**, *420*, 382−386.
(17) Fampiou, I.; Ramasubramaniam, A. Binding of Pt Nanoclusters to Point Defects in Graphene: Adsorption, Morphology, and Electronic Structure. *J. Phys. Chem C* **2012**, *116*, 6543.
(18) Acharya, C. K.; Sullivan, D. I.; Turner, C. H. Characterizing the Interaction of Pt and PtRu Clusters with Boron-Doped, Nitrogen-Doped, and Activated Carbon: Density Functional Theory Calculations and Parameterization. *J. Phys. Chem. C* **2008**, *112*, 13607−13622.
(19) Wang, J.; Lv, Y.; Li, X.; Dong, M. Point-Defect Mediated Bonding of Pt Clusters on (5,5) Carbon Nanotubes. *J. Phys. Chem. C* **2009**, *113*, 890−893.
(20) Lim, D.-H.; Wilcox, J. DFT-Based Study on Oxygen Adsorption on Defective Graphene-Supported Pt Nanoparticles. *J. Phys. Chem. C* **2011**, *115*, 22742−22747.
(21) Chi, D. H.; Cuong, N. T.; Tuan, N. A.; Kim, Y.-T.; Bao, H. T.; Mitani, T.; Ozaki, T.; Nagao, H. Electronic Structures of Pt Clusters Adsorbed on (5,5) Single Wall Carbon Nanotube. *Chem. Phys. Lett.* **2006**, *432*, 213−217.
(22) Perdew, J. P.; Burke, K.; Ernzerhof, M. Generalized Gradient Approximation Made Simple. *Phys. Rev. Lett.* **1996**, *77*, 3865−3868.
(23) Methfessel, M.; Paxton, A. T. High-precision Sampling for Brillouin-zone Integration in Metals. *Phys. Rev. B* **1989**, *40*, 3616−3621.
(24) Kresse, G.; Furthmüller, J. Efficiency of Abinitio Total Energy Calculations for Metals and Semiconductors Using a Plane-wave Basis Set. *J. Comput. Mater. Sci.* **1996**, *6*, 15−50.
(25) Kresse, G.; Furthmüller, J. Efficient Iterative Schemes for *Ab Initio* Total-energy Calculations Using a Plane-wave Basis Set. *Phys. Rev. B* **1996**, *54*, 11169−11186.
(26) Blöchl, P. E. Projector Augmented-wave Method. *Phys. Rev. B* **1994**, *50*, 17953−17979.
(27) Kresse, G.; Joubert, D. From Ultrasoft Pseudopotentials to the Projector Augmented-wave Method. *Phys. Rev. B* **1999**, *59*, 1758−1775.
(28) Creighan, S. C; Mukerji, R. J.; Bolina, A. S.; Lewis, D. W.; Brown, W. A. The Adsorption of CO on the Stepped Pt(211) Surface: A Comparison of Theory and Experiment. *Catal. Lett.* **2003**, *88*, 39−45.
(29) Karmazyn, A. D.; Fiorin, V.; Jenkins, S. J.; King, D. A. First-principles Theory and Microcalorimetry of CO Adsorption on the 211 Surfaces of Pt and Ni. *Surf. Sci.* **2003**, *538*, 171−183.
(30) Orita, H.; Inada, Y. DFT Investigation of CO Adsorption on Pt(211) and Pt(311) Surfaces from Low to High Coverage. *J. Phys. Chem. B* **2005**, *109*, 22469−22475.
(31) Yamagishi, S.; Fujimoto, T.; Inada, Y.; Orita, H. Studies of CO Adsorption on Pt(100), Pt(410), and Pt(110) Surfaces using Density Functional Theory. *J. Phys. Chem. B* **2005**, *109*, 8899−8908.
(32) Hammer, B.; Nørskov, J. K. Electronic Factors Determining the Reactivity of Metal Surfaces. *Surf. Sci.* **1995**, *343*, 211−220.
(33) Hammer, B.; Nørskov, J. K. Theoretical Surface Science and Catalysis − Calculations and Concepts. *Adv. Catal.* **2000**, *45*, 7−129.
(34) Hammer, B.; Nørskov, J. K. Why Gold is the Noblest of all the Metals? *Nature* **1995**, *376*, 238−240.
(35) Greeley, J.; Nørskov, J. K.; Mavrikakis, M. Electronic Structure and Catalysis on Metal Surfaces. *Annu. Rev. Phys. Chem.* **2002**, *53*, 319−348.
(36) Bader, R. F. W. A Quantum Theory of Molecular Structure and Its Applications. *Chem. Rev.* **1991**, *91*, 893−928.
(37) Henkelman, G.; Arnaldsson, A.; Jónsson, H. A Fast and Robust Algorithm for Bader Decomposition of Charge Densityader Decomposition of Charge Density. *Comput. Mater. Sci.* **2006**, *36*, 254−360.
(38) Alavi, A.; Hu, P.; Deutsch, T.; Silvestrelli, P. L.; Hutter, C. O. Oxidation on Pt(111): An *Ab Initio* Density Functional Theory Study. *Phys. Rev. Lett.* **1998**, *80*, 3650−3653.
(39) Philipsen, P. H. T.; van Lenthe, E.; Snijders, J. G.; Baerends, E. J. Relativistic Calculations on the Adsorption of CO on the (111) Surfaces of Ni, Pd, and Pt within the Zeroth−order Regular Approximation. *Phys. Rev. B* **1997**, *56*, 13556−13562.
(40) Hammer, B.; Morikawa, Y.; Nørskov, J. K. CO Chemisorption at Metal Surfaces and Overlayers. *Phys. Rev. Lett.* **1996**, *76*, 2141−2144.
(41) Jennison, D. R.; Schultz, P. A.; Sears, M. P. Ab Initio Ammonia and CO Lateral Interactions on Pt (111). *Phys. Rev. Lett.* **1996**, *77*, 4828−4831.
(42) Curulla, D.; Clotet, A.; Ricart, J. M.; Illas, F. Ab Initio Cluster Model Study of Chemisorption of CO on Low−Index Platinum Surfaces. *J. Phys.Chem. B* **1999**, *103*, 5246−5255.
(43) Ohnishi, S.; Watari, N. Cluster-model Study of CO Adsorption on the Pt(111) Surface. *Phys. Rev. B* **1994**, *49*, 14619−14627.
(44) Hammer, B.; Nielsen, O. H.; Nørskov, J. K. Structure Sensitivity in Adsorption: CO Interaction with Stepped and Reconstructed Pt Surfaces. *Catal. Lett.* **1997**, *46*, 31−35.
(45) Yeo, Y. Y.; Vattuone, L.; King, D. A. Calorimetric Heats for CO and Oxygen Adsorption and for the Catalytic CO Oxidation Reaction on Pt (111). *J. Chem. Phys.* **1997**, *106*, 392−401.

(46) The on-top site of the Pt(111) surface is the favored CO-adsorption site in reality, whereas DFT prefers adsorption at an FCC hollow site.[38−44] The DFT binding energy at the FCC hollow (1.80 eV) though is quite close to the experimental binding energy at the on-top site (1.68 ± 0.12 eV[45]).

dx.doi.org/10.1021/jp403468h | J. Phys. Chem. C 2013, 117, 19927−19933